molbank

MDPI

Short Note

Ammonium Aminomethylphosphonate Monohydrate

Simone Murgia [1,*], M. Carla Aragoni [1], Vito Lippolis [1,2], Enrico Podda [1,2,*], Riccardo Serra [1] and Massimiliano Arca [1]

[1] Dipartimento di Scienze Chimiche e Geologiche, Università Degli Studi di Cagliari, S.S. 554 Bivio Sestu, 09042 Monserrato (Cagliari), Italy; aragoni@unica.it (M.C.A.); lippolis@unica.it (V.L.); riccardo.serra3@unica.it (R.S.); marca@unica.it (M.A.)

[2] Centro Servizi di Ateneo per la Ricerca (CeSAR), Università Degli Studi di Cagliari, S.S. 554 Bivio Sestu, 09042 Monserrato (Cagliari), Italy

* Correspondence: simone.murgia@unica.it (S.M.); enrico.podda@unica.it (E.P.)

Abstract

Ammonium aminomethylphosphonate monohydrate was synthesized via aqueous neutralization of aminomethylphosphonic acid with ammonium carbonate. The compound was fully characterized by FT-IR and NMR spectroscopy, as well as single-crystal X-ray diffraction (SC-XRD). Structural analysis confirmed the zwitterionic nature of the aminomethylphosphonate anion and revealed an extensive 3D supramolecular network of charge-assisted N–H···O and O–H···O hydrogen bonds.

Keywords: aminomethylphosphonate; phosphonates; hydrogen bonding; SC-XRD

1. Introduction

Among organophosphorus compounds, phosphonates featuring a robust C–P bond have drawn significant attention due to their exceptional hydrolytic and thermal stability compared to classical phosphates [1–5]. While phosphates are prone to hydrolysis at the phosphorus centre [6,7], the direct P–C bond in phosphonic acids renders them extraordinarily resistant to degradation even under harsh conditions [4,7]. Consequently, substituted phosphonate derivatives serve as versatile building blocks in coordination chemistry, materials science, and crystal engineering, playing a key role in the design of functional solid-state, bioactive, and proton-conducting materials [8–13]. Very recently, ammonium hydrogen phenylphosphonate was reported as an effective consolidant for stone substrates [14].

The formation of ammonium salts from phosphonic acids via acid–base neutralization with ammonia or basic ammonium salts (such as ammonium carbonate) provides highly water-soluble crystalline solids with well-defined stoichiometries [14–16]. However, the pronounced tendency of these species to undergo self-assembly and nucleate extended crystalline domains directly affects interfacial packing, molecular organization, and the resulting performance of the modified materials, making a detailed structural understanding of their solid-state hydration and hydrogen-bonding networks essential.

The crystal structure of anhydrous ammonium aminomethylphosphonate (**1**) was recently reported in 2025 by Hu et al. [13]. Herein, we report the synthesis, spectroscopic characterization, and single-crystal X-ray structure (SC-XRD) of ammonium aminomethylphosphonate monohydrate (**1**·H_2O). A comparative structural analysis is also presented with respect to the previously reported anhydrous phase [13].

Check for updates

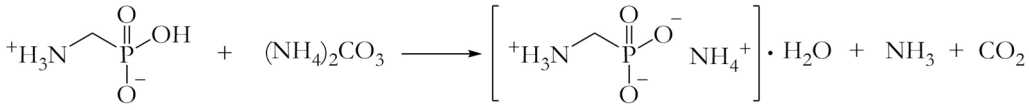
Academic Editor: Kristof Van Hecke

Received: 5 October 2026
Revised: 30 October 2026
Accepted: 3 November 2026
Published: 5 November 2026

Copyright: © 2026 by the authors. Licensee MDPI, Basel, Switzerland. This article is an open access article distributed under the terms and conditions of the Creative Commons Attribution (CC BY) license.

2. Results and Discussion

Ammonium aminomethylphosphonate monohydrate (**1**·H_2O) was synthesized in water by neutralization of aminomethylphosphonic acid with ammonium carbonate in 1:1 molar ratio (Scheme 1). Interestingly, anhydrous compound **1** was obtained from the same starting reagent under different evaporation conditions of the reaction mixture [13]. The starting aminomethylphosphonic acid is a polyprotic acid with pK_a values of 1.8, 5.4, and 10.0, the latter constant referring to the terminal amino group [17]. Hence, under neutral and acidic conditions, the amino group is protonated, and the formally neutral acid displays a zwitterionic structure [18].



1

Scheme 1. Synthesis of ammonium aminomethylphosphonate monohydrate (**1**·H_2O) by neutralization of aminomethylphosphonic acid with ammonium carbonate.

Compound **1**·H_2O was obtained as a white crystalline solid that, similarly to the starting acid [18] and other aminophosphonic compounds [19,20], showed a pronounced tendency to crystallize, readily affording large, well-defined colourless single crystals up to several millimetres in size, exhibiting varying crystal habits (Figure S1). It is worth noting that the synthesis of **1**·H_2O utilizes the same precursor as that previously reported for the anhydrous phase **1** [13], differing in the solvent evaporation process. While evaporation at 50 °C was reported to yield the known anhydrous salt **1** [13], slow room-temperature evaporation of the aqueous solution for 7 days afforded crystals of the monohydrate phase **1**·H_2O.

Compound **1**·H_2O was characterized by means of ^{1}H, ^{13}C, and ^{31}P NMR in D_2O (Figures S2–S4), showing the expected signals (^{1}H NMR: 2.77 ppm (d, $^{2}J_{P-H}$ = 12.0 Hz, CH_2); $^{13}C\{^{1}H\}$ NMR: 37.21 ppm (d, $^{1}J_{P-C}$ = 133.2 Hz); ^{31}P NMR: 9.27 ppm (t, $^{2}J_{P-H}$ = 12.0 Hz, P–CH_2). The FT-IR spectrum (Figure S5) displays a broad high-frequency absorption, with bands at 3419 and 3108 cm^{-1} assigned mainly to the O–H stretching vibration of lattice water and to overlapping N–H stretching vibrations of the ammonium cation and protonated amino group, respectively [21]. The weak bands at 2917 and 2848 cm^{-1} are consistent with the asymmetric and symmetric CH_2 stretching vibrations, respectively [21]. In the fingerprint region, the strong absorptions at 1064 and 727 cm^{-1} are consistent with P–O and P–C stretching modes of the phosphonate group, respectively [21,22]. The thermal stability and dehydration behaviour of **1**·H_2O were evaluated by simultaneous thermogravimetric and differential thermal analysis (TGA-DTA) under a dry air atmosphere up to 500 °C (Figure S6). The TGA curve exhibits an initial weight loss of ~10%–12% between room temperature and 130 °C, accompanied by an endothermic event in the DTA curve. This weight loss matches the theoretical value of 12.3% calculated for the removal of one lattice water molecule per unit formula, thereby confirming the 1:1 stoichiometry **1**·H_2O (see below). Upon dehydration, the resulting anhydrous intermediate remains stable up to approximately 180 °C, above which oxidative thermal decomposition of the organic framework takes place.

The crystal structure of **1**·H_2O was elucidated by single-crystal X-ray diffraction analysis, confirming the expected zwitterionic nature of the aminomethylphosphonate monoanion. The asymmetric unit comprises one ammonium cation, one aminomethylphosphonate monoanion, and a cocrystallized water molecule (Figure 1).

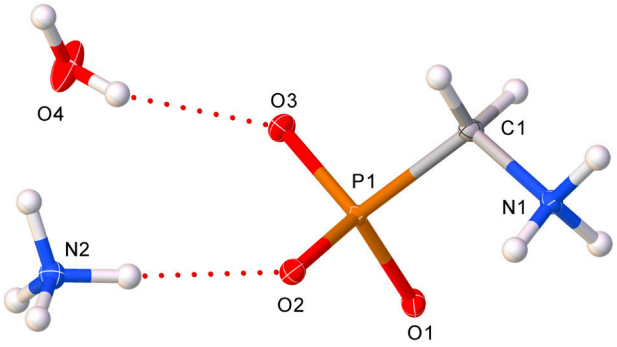


Figure 1. Ellipsoid plot of the asymmetric unit of compound **1**·H_2O viewed along the [110] crystallographic direction and showing the atom-numbering scheme. Displacement ellipsoids are drawn at the 50% probability level.

Crystal data for $CH_{11}N_2O_4P$ (M = 146.09 g mol^{-1}): monoclinic, $P2_1/n$, a = 5.8812(2) Å, b = 6.0995(2) Å, c = 18.2584(5) Å, β = 95.5880(10)°, V = 651.86(4) Å^3, Z = 4, T = 100(2) K, μ(Mo Kα) = 0.367 mm^{-1}, 16401 measured reflections, 1831 independent reflections (Rint = 0.0460, Rsigma = 0.0240), R1 = 0.0234 [I ≥ 2σ(I)] and wR2 = 0.0610 (all data).

Crystallographic data, selected bond lengths and angles are provided in Tables S1 and S2 in the Supporting Information.

The crystal packing of **1**·H_2O is sustained by an extensive three-dimensional network comprising nine crystallographically distinct charge-assisted N–H···O and O–H···O hydrogen bonds (Table 1 and Figure 2). The protonated amino group of the aminomethylphosphonate anion (N1) acts as a donor through three hydrogen bonds with phosphonate O1 and O2 acceptors belonging to three neighbouring anions (interactions a–c). The ammonium cation (N2) uses all four N–H groups as donors: three interact with phosphonate O2 and O3 atoms (interactions d–f), while the fourth forms an N–H···O contact with the cocrystallized water molecule (interaction g). The water molecule therefore acts as both a hydrogen-bond acceptor, in g, and a donor, forming two O–H···O contacts with phosphonate O2 and O3 atoms (interactions h and i, respectively). Overall, the D···A and H···A distances lie in the ranges 2.7336(12)–2.8196(12) and 1.815(14)–2.04(2) Å, respectively, with D–H···A angles ranging from 158.0(11) to 179.5(18)°.

Table 1. Hydrogen bonding interactions found in compound **1**·H_2O.

	D−H···A	**D···A (Å)**	**D−H (Å)**	**H···A (Å)**	**∠$_{D-H\cdots A}$(°)**
a	N1−H1A···O1 [i]	2.7668(11)	0.889(18)	1.880(18)	175.8(12)
b	N1−H1B···O2 [ii]	2.7336(12)	0.920(14)	1.815(14)	176.2(11)
c	N1−H1C···O1 [iii]	2.8124(12)	0.872(12)	1.984(12)	158.0(11)
d	N2−H2A···O2	2.7967(11)	0.898(17)	1.915(17)	166.7(17)
e	N2−H2B···O3 [iv]	2.7828(12)	0.889(18)	1.921(18)	163.0(17)
f	N2−H2C···O3 [v]	2.8196(12)	0.906(19)	1.931(19)	166.2(16)
g	N2−H2D···O4 [vi]	2.7445(13)	0.864(18)	1.881(18)	178.3(17)
h	O4−H4A···O2 [v]	2.7443(12)	0.853(19)	1.891(19)	179.5(18)
i	O4−H4B···O3	2.7558(12)	0.74(2)	2.04(2)	161.2(2)

[i] = 1 + x, +y, +z; [ii] = 3/2−x, −1/2 + y, 3/2 − z; [iii] = 3/2 − x, ½ + y, 3/2 − z; [iv] = +x, 1 + y, +z; [v] = 1 − x, 1 − y, 1 − z; [vi] = −x, 1 − y, 1 − z.

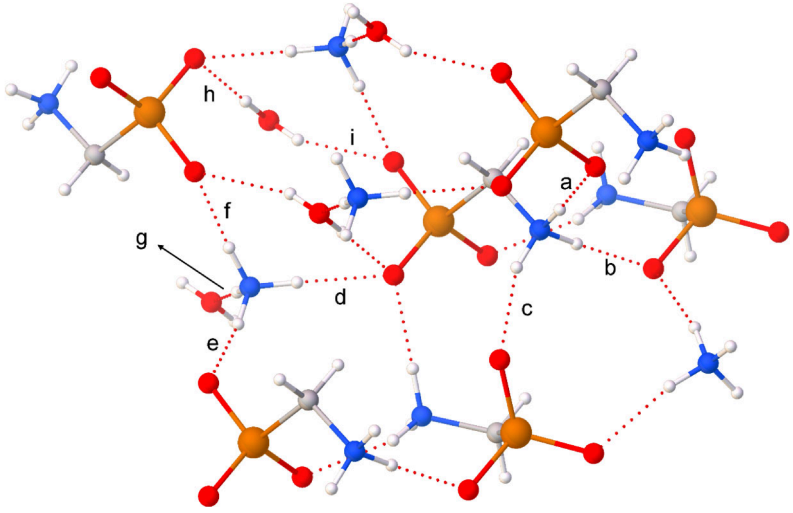


Figure 2. Hydrogen bonding interactions in **1**·H_2O. Interactions are labelled according to Table 1.

Graph-set analysis reveals four recurrent ring motifs within the hydrogen-bonded framework [23,24]. Interactions b and c generate $R_2^2(10)$ rings and, together with interactions d and e, give rise to $R_4^3(10)$ motifs. Interactions d, f, h, and i define $R_4^2(8)$ rings, whereas two symmetry-related pairs of the water-mediated interactions h and i generate $R_4^4(12)$ rings. Representative examples of these motifs are shown schematically in Figure S7. These rings are interconnected through the remaining hydrogen bonds, producing the extended three-dimensional network. Interestingly, the $R_2^2(10)$ and $R_4^3(10)$ motifs are also present in the previously reported anhydrous phase **1**, as identified by graph-set analysis of the deposited crystal structure of Hu et al. [13]. In contrast, the $R_4^2(8)$ and $R_4^4(12)$ rings observed in **1**·H_2O involve the lattice water molecule and are therefore specific to the hydrated form. Hydration thus preserves part of the hydrogen-bonding topology of the anhydrous phase while introducing additional water-mediated ring motifs that reorganize the connectivity of the three-dimensional framework.

3. Materials and Methods

3.1. General Methods

All reagents were purchased from Merck (Darmstadt, Germany) and used without further purification. FT-IR spectra (KBr beam splitter, KBr windows, 4000–400 cm^{-1}, resolution 4 cm^{-1}) were recorded on a Thermo-Nicolet 5700 spectrometer (Madison, WI, USA) at room temperature on KBr pellets of the analysed samples. ^1H NMR and ^{31}P NMR measurements were carried out in D_2O at 25 °C, using a Bruker Avance III HD spectrometer (Rheinstetten, Germany) (14.1 T), operating at 600 and 243 MHz, respectively. Chemical shifts are reported in ppm (δ). TGA measurements were performed using a Perkin Elmer STA 6000 Simultaneous Thermal Analyser (Shelton, CT, USA). 10 mg of sample were weighed on an alumina crucible and a curve from 25 to 500 °C with a gradient of 10 °C per min using a 40 mL min^{-1} dry air flow was recorded.

3.2. X-Ray Diffraction Analysis

Single-crystal X-ray diffraction data for compound **1**·H_2O were collected at 100 K on a Bruker D8 Venture diffractometer (Karlsruhe, Germany) equipped with a PHOTON II CPAD detector (Karlsruhe, Germany) and a Mo Kα radiation (λ = 0.71073 Å) generated by an Incoatec IμS microfocus X-ray source (Geesthacht, Germany), operated at 50 kV and 1.0 mA. The structure was solved with SHELXT [25] using dual-space methods and refined using SHELXL [26] through cycles of least-squares refinement of F^2. Hydrogen atoms

bonded to carbon were placed in geometrically calculated positions and refined using a riding model, with $U_{iso}(H) = 1.2U_{eq}(C)$. Hydrogen atoms on heteroatoms were located from the difference Fourier map and refined freely.

*3.3. Synthesis of Ammonium Aminomethylphosphonate Monohydrate (**1**·H_2O)*

Aminomethylphosphonic acid (0.55 g, 5.0 mmol) dissolved in 200 mL of water was slowly added to 0.48 g (5.0 mmol) of ammonium carbonate dissolved in 50 mL of water. The resulting solution was stirred for 3 h and subsequently transferred to a crystallizer. The solvent was allowed to evaporate in 7 days at atmospheric pressure at r.t., in a laboratory conditioned at 24 ± 2 °C, affording colourless crystals. Yield: 0.6105 g, 84%. FT-IR (KBr pellet) ν = 3419 (m), 3108 (w), 2917 (vw), 2848 (vw), 2616 (w), 1623 (m), 1527 (m), 1442 (m), 1301 (w), 1195 (vw), 1130 (vw), 1093 (vw), 1064 (vs), 975 (w), 929 (w), 819 (w), 727 (s), 470 (m) cm^{-1}. ^1H NMR (600 MHz, D_2O) δ = 2.77 ppm (d, $^2J_{P-H}$ = 12.0 Hz, 2H, CH_2). $^{13}C\{^1H\}$ NMR (151 MHz, D_2O) δ = 37.21 (d, $^1J_{P-C}$ = 133.2 Hz) ppm. ^{31}P NMR (243 MHz, D_2O) δ = 9.27 ppm (t, $^2J_{P-H}$ = 12.0 Hz, 1P).

4. Conclusions

In conclusion, we have determined the spectroscopic properties and crystal structure of ammonium aminomethylphosphonate monohydrate (**1**·H_2O). The solid-state architectures of both the anhydrous and monohydrate phases are governed by intricate hydrogen-bonding networks involving the ammonium cations, the zwitterionic anions, and, in the case of **1**·H_2O, co-crystallized water molecules. While the marked propensity of these species to form extended supramolecular networks and large crystalline domains highlights their structural robustness, it also suggests potential limitations for direct application as stone consolidants. In particular, excessive crystal growth within the pore system of stone substrates could potentially induce crystallization stress. Nevertheless, understanding these fundamental assembly mechanisms remains essential for tailoring soluble ammonium phosphonate precursors toward optimized conservation treatments.

Supplementary Materials: The following supporting information can be downloaded online. Figure S1: Representative single crystals of compound **1**·H_2O obtained from aqueous solution (scale ruler in cm); Figure S2. Portion of the ^1H NMR spectrum recorded on a D_2O solution of compound **1**·H_2O; Figure S3. Portion of the ^{31}P NMR spectrum recorded on a D_2O solution of compound **1**·H_2O; Figure S4. Portion of the $^{13}C\{^1H\}$ NMR spectrum recorded on a D_2O solution of compound **1**·H_2O; Figure S5. Solid state FT-IR spectrum recorded for compound **1**·H_2O (KBr pellet); Figure S6. TGA (black line) and DTA (red line) curves of **1**·H_2O recorded under a dry air atmosphere (25–500 °C). Figure S7: Schematic representation of selected hydrogen-bonded ring motifs identified by graph-set analysis in the crystal structure of compound **1**·H_2O. Table S1: Crystal data and structure refinement parameters for compound **1**·H_2O; Table S2: Bond lengths (Å) and angles (°) for compound **1**·H_2O.

Author Contributions: Conceptualization: M.A. Methodology: M.A., M.C.A. and V.L. Investigation: S.M., R.S. and E.P. Data curation: S.M. and E.P. Writing—original draft preparation: S.M. and M.A. Writing—review and editing: M.C.A., R.S., V.L. and E.P. All authors have read and agreed to the published version of the manuscript.

Funding: This research was funded by Fondazione di Sardegna (FdS Progetti Biennali di Ateneo, annualità 2024–2025, F83C26000350007).

Data Availability Statement: Crystallographic data were deposited at CCDC with deposition number 2589784. These data can be obtained free of charge from the CCDC via https://www.ccdc.cam.ac.uk/structures (accessed on 1 October 2026). Additional data supporting the findings of this study are available from the corresponding author upon reasonable request.

Acknowledgments: CeSAR (Centro Servizi di Ateneo per la Ricerca) of the University of Cagliari is acknowledged for XRD and NMR facilities.

Conflicts of Interest: The authors declare no conflicts of interest.

References

1. Kristensen, P. Recent advances in the synthesis of organophosphorus chemistry and its use in pharmacological formulations. *Org. Chem. Curr. Res.* **2023**, *12*, 302. [CrossRef]
2. Büchel, K.H.; Moretto, H.-H.; Woditsch, P. *Industrial Inorganic Chemistry*, 2nd ed.; Wiley-VCH: Weinheim, Germany, 2000. [CrossRef]
3. Montchamp, J.-L. Phosphinate chemistry in the 21st century: A viable alternative to the use of phosphorus trichloride in organophosphorus synthesis. *Acc. Chem. Res.* **2014**, *47*, 77–87. [CrossRef] [PubMed]
4. Metcalf, W.W.; van der Donk, W.A. Biosynthesis of phosphonic and phosphinic acid natural products. *Annu. Rev. Biochem.* **2009**, *78*, 65–94. [CrossRef] [PubMed]
5. Schartel, B. Phosphorus-based flame retardancy mechanisms—Old hat or a starting point for future development? *Materials* **2010**, *3*, 4710–4745. [CrossRef] [PubMed]
6. Kerr, J.A. Strengths of chemical bonds. In *CRC Handbook of Chemistry and Physics*, 81st ed.; Lide, D.R., Ed.; CRC Press: Boca Raton, FL, USA, 2000; ISBN 978-0-8493-0481-1.
7. Harsági, N.; Keglevich, G. The hydrolysis of phosphinates and phosphonates: A review. *Molecules* **2021**, *26*, 2840. [CrossRef] [PubMed]
8. Perez, O.; Bloyet, C.; Rueff, J.-M.; Barrier, N.; Jaffrès, V.; Raveau, P.-A. Topochemical route from supramolecular to hybrid materials: Tetraphenylmethane-based tectons and lanthanum phosphonate derivative. *Cryst. Growth Des.* **2016**, *16*, 6781–6789. [CrossRef]
9. Biasone, A.; Tortorella, P.; Campestre, C.; Agamennone, M.; Preziuso, S.; Chiappini, M.; Nuti, E.; Carelli, P.; Rossello, A.; Mazza, F.; et al. α-Biphenylsulfonylamino 2-methylpropyl phosphonates: Enantioselective synthesis and selective inhibition of MMPs. *Bioorg. Med. Chem.* **2007**, *15*, 791–799. [CrossRef] [PubMed]
10. Dang, Q.; Brown, B.S.; Liu, Y.; Rydzewski, R.M.; Robinson, E.D.; van Poelje, P.D.; Reddy, M.R.; Erion, M.D. Fructose-1,6-bisphosphatase inhibitors. 1. Purine phosphonic acids as novel AMP mimics. *J. Med. Chem.* **2009**, *52*, 2880–2898. [CrossRef] [PubMed]
11. Graillot, A.; Djenadi, S.; Faur, C.; Bouyer, D.; Monge, S.; Robin, J.-J. Removal of metal ions from aqueous effluents involving new thermosensitive polymeric sorbent. *Water Sci. Technol.* **2013**, *67*, 1181–1187. [CrossRef] [PubMed]
12. Kim, M.-J.; Jeon, I.-Y.; Seo, J.-M.; Dai, L.; Baek, J.-B. Graphene phosphonic acid as an efficient flame retardant. *ACS Nano* **2014**, *8*, 2820–2825. [CrossRef] [PubMed]
13. Hu, C.; Qu, J.; Hu, J.; Liu, J.; Hu, W.; Jiang, X. $NH_4PO_3HCH_3$ and $NH_4PO_3CH_2NH_3$: Two phosphate derivatives with deep-UV cutoff edges and moderate birefringence. *Inorg. Chem.* **2025**, *64*, 9356–9363. [CrossRef] [PubMed]
14. Murgia, S.; Aragoni, M.C.; Carcangiu, G.; Coles, S.J.; Columbu, S.; Ennas, G.; Lippolis, V.; Meloni, P.; Navarro Ezquerra, A.; Orton, J.B.; et al. Protecting white Carrara marble with organophosphorus salts: A case study of ammonium hydrogen phenylphosphonate. *Mater. Adv.* **2026**, *7*, 2180–2194. [CrossRef]
15. Wakeman, R.L.; Coates, J.F. Quaternary Ammonium Salts of Organophosphorus Acids. U.S. Patent 3,280,131, 18 October 1966. Available online: https://patents.google.com/patent/US3280131A/en (accessed on 2 November 2026).
16. Ding, D.; Liu, Y.; Lu, Y.; Liao, Y.; Chen, Y.; Zhang, G.; Zhang, F. Highly effective and durable P–N synergistic flame retardant containing ammonium phosphate and phosphonate for cotton fabrics. *Polym. Degrad. Stab.* **2022**, *200*, 109964. [CrossRef]
17. Chen, Z.; He, W.; Beer, M.; Megharaj, M.; Naidu, R. Speciation of glyphosate, phosphate and aminomethylphosphonic acid in soil extracts by ion chromatography with inductively coupled plasma mass spectrometry with an octopole reaction system. *Talanta* **2009**, *78*, 852–856. [CrossRef] [PubMed]
18. Janicki, R.; Starynowicz, P. Charge density distribution in aminomethylphosphonic acid. *Acta Crystallogr. Sect. B Struct. Sci.* **2010**, *66*, 559–567. [CrossRef] [PubMed]
19. Okaya, Y. Crystal structure of the stable modification of 2-aminoethylphosphonic acid, β-ciliatine. *Acta Crystallogr.* **1966**, *20*, 712–715. [CrossRef]
20. Schmidt, C.; Feyand, M.; Rothkirch, A.; Stock, N. High-throughput and in situ EDXRD investigation on the formation of two new metal aminoethylphosphonates—$Ca(O_3PC_2H_4NH_2)$ and $Ca(OH)(O_3PC_2H_4NH_3)\cdot 2H_2O$. *J. Solid State Chem.* **2012**, *188*, 44–49. [CrossRef]
21. Socrates, G. *Infrared and Raman Characteristic Group Frequencies: Tables and Charts*, 3rd ed.; John Wiley & Sons: Chichester, UK, 2001; ISBN 0-471-85298-8.
22. Corbridge, D.E.C. Infra-red analysis of phosphorus compounds. *J. Appl. Chem.* **1956**, *6*, 456–465. [CrossRef]

23. Bernstein, J.; Davis, R.E.; Shimoni, L.; Chang, N.-L. Patterns in hydrogen bonding: Functionality and graph-set analysis in crystals. *Angew. Chem. Int. Ed. Engl.* **1995**, *34*, 1555–1573. [CrossRef]
24. Etter, M.C.; MacDonald, J.C.; Bernstein, J. Graph-set analysis of hydrogen-bond patterns in organic crystals. *Acta Crystallogr. Sect. B Struct. Sci.* **1990**, *46*, 256–262. [CrossRef] [PubMed]
25. Sheldrick, G.M. SHELXT—Integrated space-group and crystal-structure determination. *Acta Crystallogr. Sect. A Found. Adv.* **2015**, *71*, 3–8. [CrossRef] [PubMed]
26. Sheldrick, G.M. Crystal structure refinement with SHELXL. *Acta Crystallogr. Sect. C Struct. Chem.* **2015**, *71*, 3–8. [CrossRef]

Disclaimer/Publisher's Note: The statements, opinions and data contained in all publications are solely those of the individual author(s) and contributor(s) and not of MDPI and/or the editor(s). MDPI and/or the editor(s) disclaim responsibility for any injury to people or property resulting from any ideas, methods, instructions or products referred to in the content.